Heliyon 8 (2022) e10502

Contents lists available at ScienceDirect

Heliyon

journal homepage: www.cell.com/heliyon

Research article

Mechanical and microstructural properties of high-performance concrete made with rice husk ash internally cured with superabsorbent polymers

David O. Nduka [a,*], Babatunde J. Olawuyi [c], Emmanuel O. Fagbenle [b], Belén G. Fonteboa [d]

[a] Department of Building Technology; College of Science and Technology, Km 10 Idiroko Road, Covenant University, Ota, Ogun State, Nigeria
[b] Department of Civil Engineering; College of Engineering, Km 10 Idiroko Road, Covenant University, Ota, Ogun State, Nigeria
[c] Department of Building, School of Environmental Technology, Federal University of Technology, Minna, Nigeria
[d] Department of Civil Engineering, School of Civil Engineering, University of A Coruña, Spain

ARTICLE INFO

Keywords:
High-performance concrete
Rice husk ash
Superabsorbent polymers
Internal curing
Microstructure and mechanical properties

ABSTRACT

An experimental study was carried out to determine the properties of rice husk ash (RHA) and its effect on high-performance concrete's (HPC) mechanical and microstructural properties. RHA content was placed at 0–30% at 5% step intervals and a constant water-binder ratio (W/B) of 0.3. A slump flow test was carried out to measure the workability property of the fresh HPC. In contrast, the influence of RHA contents on compressive, splitting tensile, flexural strengths and microstructural properties were examined for the hardened HPC specimens. The X-ray fluorescence (XRF), scanning electron microscopy-energy dispersive x-ray (SEM-EDX), X-ray diffraction (XRD), Fourier-transform infrared spectroscopy-Attenuate total reflectance (FTIR-ATR), Thermogravimetry analysis (TGA), Brunauer, Emmett and Teller (BET) specific surface area and laser diffraction particle size distribution (PSD) were used to access the feasibility of RHA in HPC. XRD and SEM/EDX techniques were conducted to investigate the hydration products and microstructure in hardened HPCs. The post-test examination showed increased compressive, splitting tensile and flexural strengths of HPC samples for a 10% RHA content mix, recording the highest compressive strength in all curing ages. As the curing ages increase, the microstructure of the samples with RHA becomes denser than the control due to the refinement of the microstructure by the RHA incorporated. The XRD and SEM/EDX confirmed the lower calcium hydroxides from pozzolanic reactivity and later formation of C–S–H. The results suggest that RHA can be used as a cement replacement for up to 10% in HPC to produce sustainable concrete.

1. Introduction

High-performance concrete (HPC) is typically defined as concrete with enhanced performance in terms of strength, workability, and durability that cannot be achieved with conventional materials using standard mixing, placing, and curing procedures (American Concrete Institute, ACI, 1999; Neville, 2012; Aitcin, 2004; Faleschini et al., 2015; Biskri et al., 2017). With the addition of one or more supplementary cementitious materials (SCMs) such as silica fume (SF), fly ash (FA), ground granulated blast furnace slag (GGBS), metakaolin (MK), and rice husk ash (RHA) etc., HPC contains more cement than normal strength concrete (NSC). It is accomplished by reducing the water-to-binder ratio (W/B) to between 0.2 and 0.4, modifying the pore structure and microstructure of cement paste with SCMs, and enhancing workability with a high dosage of superplasticizer (Faleschini et al., 2015; Harbec et al., 2017). Utilised materials are typically carefully selected, high-quality constituents with an optimised mix design. The aggregates should be robust, durable, and compatible with cement paste in rigidity and strength (Aitcin, 2004).

Undoubtedly, cement is one of the most vital ingredients in HPC production, providing binding capabilities to the mixture. However, the setbacks of cement lie in the high energy demand and clinker's calcination high temperatures of about 1450 °C with the attendant effect of greenhouse gases like carbon dioxide (CO_2) emission of 0.85 ton per 1 ton of cement manufacturing (Tulashie et al., 2021). Reports have estimated clinker's annual global CO_2 emissions to be 5–8% (Afroughsabet et al., 2021), making it the second-largest contributor of CO_2 emissions after the power generation industry (Wi et al., 2018). In this light, concerted efforts have been made by researchers and practitioners toward the development of SCMs and incorporating them into concrete

* Corresponding author.
E-mail address: david.nduka@covenantuniversity.edu.ng (D.O. Nduka).

https://doi.org/10.1016/j.heliyon.2022.e10502
Received 6 June 2021; Received in revised form 17 March 2022; Accepted 25 August 2022

production. For example, Sandhu and Siddique (2017) found that SCMs in cement and concrete applications lowered heat of hydration, increased strength, decreased permeability at higher amounts, enhanced chloride and sulphate resistance/mild acids, lesser materials costs regarding cement savings, and ecologic benefits related to waste disposal and reduced CO_2 emissions.

Unfortunately, SCMs investigators (Aitcin, 2004; Biskri et al., 2017; Scrivener et al., 2018; Jaskulski et al., 2020; Nwankwo et al., 2020) have noted the various SCMs shortfalls around the world. Scrivener et al. (2018) posit that over 80% of SCMs used in cement production come from limestone, FA, or GGBS. GGBS available worldwide is 5–10% compared to cement, while FA is about 30% higher. Biskri et al. (2017) pointed out that the inclusion of GGBS in HPC mixtures reduces hydration heat and increases permeability and porosity in binders paste with 20% maximum cement replacement. The availability of GGBS also depends on the steel industry's availability. The global concern for reducing CO_2 emissions from coal burning to produce electricity is another limiting factor to FA production (Jaskulski et al., 2020). This drawback will considerably reduce the use of FA shortly. Although limestone is abundant, adding about 10% to clinker accounts for increased porosity and reduced properties (Scrivener et al., 2018). Aitcin (2004) opined that HPC production always requires 7.5–8% SF incorporation. He argued that SF's access, economics, and service factors are relevant concerns for HPC applications (Aitcin, 2004).

Despite SF's cost, the dark grey colour affects the aesthetic appearance of the concrete product. Another limitation that Ghafari et al. (2016) observed was increased water demand due to high specific surface area, affecting flowability. In addition, the inclusion of SF requires a higher dosage of superplasticiser that makes mixtures sticky. Studies (Zhang et al., 2003; Mazloom et al., 2004; Igarashi et al., 2005), as reported in Ghafari et al. (2016), showed that the addition of SF in HPC increased autogenous shrinkage. Also, the non-availability or difficulties with importing SF in Nigeria necessitates searching for a suitable available alternative (Nduka et al., 2020). MK has been demonstrated to be the best clay for SCM production and suggested for achieving dense concrete. Still, it is limited by the plate morphology in conflict with SF's spherical morphology (Büyüköztürk and Lau, 2004). Furthermore, the low availability of high-grade MK deposits and competitive use from ceramic, refractory and paper industries poses challenges to cement and concrete industries (Almenares et al., 2017).

The above factors drive other available, affordable, and sustainable alternative SCM in Nigeria's built environment. RHA has been considered a viable alternative, with a 60% increase in rice production in Nigeria between 2013 and 2019 (Salisu et al., 2021). This scenario has given rise to the need to improve the rice production byproduct requirements. RHA is a byproduct of rice husk's controlled and uncontrolled calcination in an agro-industrial setting. According to De Sensale &Viacava (2018), the global RHA production is approximately 20 million tonnes, with the husk comprising approximately 20% of the rice paddy's weight. Twenty to twenty-five percent of the husk's total weight is recovered as ash after burning (Kaur et al., 2018). RHA is known for its low density and extremely high silica (SiO_2) content when calcined in a controlled environment. Its specific gravity ranges from 2.05 to 2.53, less than the PC's 3.50 value (Fapohunda et al., 2017). According to the findings of Fapohunda et al. (2017), the cumulative useful oxide (SiO_2+Al_2O_3+Fe_2O_3) composition of RHA calcined in a controlled incinerator is greater than 70%, meeting the requirements of Class F Pozzolan of ASTM C618 (2015). The inability of RHA in Nigeria to attain optimal pozzolanic reactivity in concrete products was attributed to substandard calcination techniques in an uncontrolled incineration facility (Olutoge and Adesina, 2019). In applications involving concrete and mortar, the incinerator's burning temperature primarily determines the amorphous state of RHA. However, RHA could address the shortfalls of SCMs in developing countries like Nigeria.

In driving the utilisation of RHA in concrete, Ambedkar et al. (2017) combined experimental and modelling techniques to investigate the effect of various particle sizes of uncontrolled calcined RHA on pozzolanic reactivity, bulk density, thermal diffusivity, and compressive strength exposed to acid and alkali attack on 25 MPa concrete with W/B of 0.45. They found that increases in fineness, bulk density and specific surface area of RHA increase compressive strength, pozzolanic activity and reduced chemical attack on RHA blended concrete. Different temperatures effect on a 20 MPa RHA blended concrete cured for up to 200 days was examined by Umasabor and Okovido (2018). Their result indicated that 5% PC replacement with RHA calcinated from 500 to 700 °C for 2 h has better compressive strength than any other mixes. Olutoge and Adesina (2019) investigated RHA calcined using open burning charcoal-powered incinerator to determine the compressive and splitting tensile strengths of binary 1:2:4 concrete mix design. Their results showed a higher compressive and splitting tensile strengths of control than the 5, 7.5,10, 12.5 and 15% PC replacement with RHA. Srinath et al. (2021) used a ternary mix containing PC, high silica (86.94%) content, grey, irregular and non-crystalline RHA with particle size >45 microns and hydrated lime in examining the mechanical properties of an eco-friendly normal strength concrete. The results revealed that PC replacement with 10% RHA+10% hydrated lime gave the best mechanical properties values among other mixes.

Earlier researchers (Chindaprasirt et al., 2007; Ganesan et al., 2008; Salas et al., 2009; Madandoust et al., 2011; Gastaldini et al., 2014; Bie et al., 2015) incorporated RHA in HPC mix at between 5 - 20% binder content with improved compressive strength and durability. However, studies in Nigeria (Alhassan, 2008; Agbede and Obam, 2008; Oyekan and Kamiyo, 2008; Dabai et al., 2009; Abalaka, 2012) replaced cement with RHA in either normal strength concrete or sandcrete block applications with little or no improvement in compressive strength recorded. Nigerian investigators' low compressive strength of concrete and sandcrete blocks may be linked to an open burning system used in calcining the RHA resulting in weak or non-reactive silica (Fapohunda et al., 2017; Olutoge and Adesina, 2019). However, the cement replacement with RHA in high-performance concrete and mortar is adjudged to improve concrete performances regarding strength, durability, and pore refinement (Nduka et al., 2020; Olawuyi et al., 2020).

Superabsorbent polymers (SAP) have spurred researchers' rising interest in cement-based materials. This interest can be seen in the number of reviewed papers on the recent progress and experimental works adding SAP in a cement-based matrix (Snoeck et al., 2015, 2021; He et al., 2019; Zhong et al., 2019, 2021; Li et al., 2020; Filho et al., 2020; Mechtcherine et al., 2021; Xu et al., 2021; Tan et al., 2021; De Meyst et al., 2021; Zhong et al., 2021a,b; Schröfl et al., 2022). In their reviews, He et al. (2019), Mechtcherine et al. (2021); Xu et al. (2021), and Schröfl et al. (2022) found that the addition of SAP in cementitious materials is beneficial for reducing plastic and autogenous shrinkages, providing self-healing and impermeability of damaging ions. In experimental works that added SAP in cementitious materials, Li et al. (2020) studied the influence of pure and modified SAPs of crosslinked polyacrylic acid and neutralised by sodium hydroxide on the healing efficiency of a high-strength mortar at varying percentages. The authors' work showed a satisfactory close crack healing efficiency of the SAP-induced cement-based materials. Snoeck et al. (2015) and Snoeck et al. (2021) empirical studies also demonstrated potassium salt polyacrylate and copolymer of acrylamide and sodium acrylate of bulk polymerisation-based SAPs reduced autogenous shrinkage in a cement-based paste. De Meyst et al. (2021) carried out swelling capacity, workability, mechanical properties, final setting time and autogenous shrinkage tests on two commercial SAPs in a cement matrix. The particle sizes of both SAPs are D_{50} of 40 μm and 100 μm, respectively, synthesised by bulk polymerization. Their study concluded that despite some negative effects of SAPs on their tested samples' workability and compressive strength, SAPs addition to cementitious matrix provided reduced autogenous shrinkage, leading to durable and appealing structures.

Furthermore, ionic and non-ionic types of SAPs based on sodium acrylate of polymer and acrylic acid of polymer were tested for

Table 1. Experimental plans.

Type	Experiment	Experimental factors
Characterisation of the RHA and CEM II	XRF, SEM-EDX, XRD, FTIR-ATR, TGA, BET, and laser PSD	RHA and CEM II powder
Effect of RHA on CEM II-based HPC	Compressive strength	Substitution ratio of RHA • (0, 5, 10, 15, 20, 25, and 30%) Curing ages • (7, 28, 56, and 90 days)
	Splitting tensile and flexural strengths	Substitution ratio of RHA • (0, 5, 10, 15, 20, 25, and 30%) Curing ages (28, 56, and 90 days)
	SEM-EDX	Substitution ratio of RHA • (0, 10, and 20%)
	XRD	Substitution ratio of RHA • (0, 10, and 20%)

absorption (tea-bag test) and compressive strength at different ages of varying percentages of SAP (Tan et al., 2021). Their result depicts that at 28 days of curing, SAP addition significantly improves the compressive strength of cement paste. Other studies (Senff et al., 2015; Oh and Choi, 2018; Yang et al., 2019; Tu et al., 2019) studied the impacts of SAP on the drying, autogenous, and mechanical shrinkage properties of concrete and mortars with W/B less than 0.40. Similar results indicate that SAP plays a crucial role in reducing the shrinkage and porosity of cement paste. Notwithstanding, studies have revealed poor mechanical properties of HPC with SAP presence (Olawuyi and Boshoff, 2017; Dushimimana et al., 2021), particularly at an early age due to the formation of voids, with strength improving with age. The voids created can be compensated by enhanced workability and freezing-thawing resistance (Ma et al., 2020). Dushimimana et al. (2021) posit that SAP addition in HPC leads to reduced porosity arising from the release of water when the relative humidity of the concrete section drops. Subsequently, a spherical or irregular-shaped "SAP void" is formed and filled by either calcium hydroxide or ettringite developed near the SAP particles. This interaction of SAP in cementitious material improved compressive strength (Nduka et al., 2020; Olawuyi et al., 2020). In addition to the laboratory results of SAP in minimising plastic and autogenous shrinkage in cementitious materials, its practical application in large-scale concrete projects has been seen. For instance, Mechtcherine et al. (2021) reported that SAP incorporation in concrete minimised shrinkages in the $20 \times 50 \times 0.85\ m^3$ concrete shear wall, $12 \times 8 \times 0.12\ m^3$ slab, $8 \times 10^5\ m^3$ railway slab, and China Zau Tower, respectively. Consequently, due to the availability of RHA in Nigeria and limited studies using this material in HPC, this paper aimed to investigate the strength and microstructural performance of HPC containing RHA as a partial replacement of cement internally cured with SAP. The present study draws on Nduka et al. (2022) that investigated the usefulness of RHA in improving the durability properties of HPC.

2. Materials and methods

2.1. Outline of experiment

An experimental plan was made to analyse the material properties of RHA and its influence on the mechanical properties and microstructure of the HPC matrix, as shown in Table 1. Initially, to understand the composition and morphology of the Portland-limestone cement (CEM II B-L, 42.5 N) and RHA, X-ray fluorescence (XRF), scanning electron microscopy-energy dispersive x-ray (SEM-EDX), X-ray diffraction (XRD), Fourier-transform infrared spectroscopy-Attenuate total reflectance (FTIR-ATR), Thermogravimetry analysis (TGA), Brunauer, Emmett and Teller (BET) specific surface area and laser diffraction particle size distribution (PSD) were applied.

After knowing their material properties, RHA was incorporated at 0–30% b_{wob} contents at a 5% steps interval, and the compressive, splitting tensile and flexural strengths of HPC samples were determined. In addition, the quantitative and qualitative analyses of the hydration products were performed using the SEM-EDX and XRD techniques.

2.2. Materials

This study used CEM II, conforming to EN, B.S. 197-1 (2011) and Nigeria Industrial Standard [NIS], 444-1 (2018). Chemical and physical characteristics are listed in Table 2. Rice husk was collected from a rice mill in Minna, Niger State, Nigeria, to produce RHA. The rice husk was calcined to ash at 700 °C for 1 h in an electric furnace and ground in a grinding mill at the Laboratory of the Nigeria Cereals Research Institute in Baddegi, Niger State, Nigeria, close to Bida. The particle size distribution (PSD) of CEM II and RHA was measured via the laser PSD method presented in Figure 1.

Masterglenium Sky 504 – a polycarboxylic ether polymer-based superplasticiser made available by BASF Limited (West Africa) was used to enhance the workability of the HPC mixtures. It was applied only within the maker's optimal specification of 2% by weight of binder (b_{wob}). The superplasticizer has a specific gravity of 1.115 and is chlorine-free.

As internal curing (IC) agent, "FLOSET 27CC $\geq$ 300 μm" SAP, as characterised in a previous publication by Olawuyi and Boshoff (2013) and Olawuyi and Boshoff (2016), was used at a constant content of 0.3% b_{wob}. The tea-bag test revealed an absorption capacity of 250 g/g in distilled water and 25 g/g in cement pore solution. The SAP particles were sealed in a plastic bag and preserved (with exposure to moisture avoided) in a wooden cabinet until use. Generally, the tea-bag test followed the protocols enshrined in the RILEM TC 260-RSC recommendations on testing absorption by SAP before implementation in cement-based materials (Snoeck et al., 2018).

2.3. Specimen preparation

Cubic, cylindrical and prismatic beams HPC samples were prepared with 100 mm cubes, Ø100 × 200 mm cylinders and 100 × 100 × 500 mm prisms, respectively, for compressive, splitting tensile and flexural

Table 2. Chemical composition and physical properties of CEM II and RHA.

Oxides	RHA (%)	CEM II (%)
SiO_2	80.02	15.38
Al_2O_3	1.81	4.14
Fe_2O_3	0.79	3.19
CaO	0.82	56.92
MgO	0.74	2.44
SO_3	0.08	1.59
K_2O	1.01	0.21
Na_2O	0.00	0.04
M_2O_5	0.26	0.04
P_2O_5	4.31	0.28
TiO_2	0.43	0.21
Loss on ignition (LOI)	10.62	15.59
$SiO_2 + Al_2O_3 + Fe_2O_3$	82.62	22.71
Total	100.89	100.03
Specific gravity	2.15	3.12
MultiPoint BET SSA (m^2/g)	4.649×10^2	8.182×10^2
Soundness (%)		0.75
Initial and final setting times (min)		90 & 205
Pore diameter mode-DA (nm)	1.52	2.92

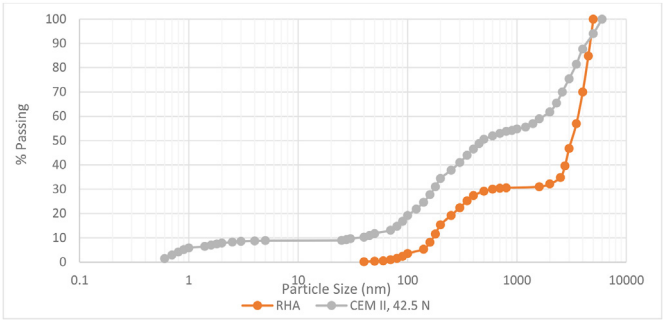

Figure 1. Particle size distribution of binders (Nduka et al., 2022).

strengths tests following EN B. 12390-3 (2019), EN B. 12390-6 (2010) and International Union of Testing and Research Laboratories for Materials and Structures, RILEM Technical Recommendation TC14-CPC 4 (1975). The mix design of HPC specimens as per the British method is shown in Table 3. The water-to-binder ratio (W/B) was kept constant at 0.3, and RHA was incorporated as 0–30% b_{wob} contents at 5% step intervals. A fixed SAP content of 0.3% b_{wob} and 1.5% b_{wob} superplasticiser content was introduced. Extra water of 12.5 g/g of SAP was added based on the SAP absorption properties established by Olawuyi's research (2016). The HPC classifications were tagged with the name of RHAC with RHA contents attached. For instance, the HPC containing RHA with 5% RHA content was coded as RHAC-5. After casting, each sample was cured at room temperature for 24 h. After demoulding, specimens were cured in water at 21 ± 2 °C till the experiment date. For the characterisation of the hydration products, XRD and SEM-EDX techniques were conducted on the remains of crushed selected HPC samples of control, 10 and 20% CEM II replacement of RHA at 90 days. XRD and SEM/EDX data were collected on 75 μm particles and a thin section of about 3 mm thick HPC samples after hydration stoppage with acetone for 24 h.

The hydration stoppage treatment was applied to the hardened RHA-blended HPC mixtures to preserve the cement hydrate in the matrix (Snellings et al., 2018). The protocol provided by the RILEM TC-238 committee on hydration stoppage by solvent exchange for studying hydrate assemblages was adhered to in preparing the samples for further characterisation. However, isopropanol was not used to preserve the cement hydrate recommended by the document due to unavailability.

2.4. Test methods

2.4.1. Characterisation of CEM II and RHA

BET (Nova Station B Quantachrome Instrument, Boynton Beach, FL, USA) and laser PSD (Malvern Mastersizer 3000, Worcestershire, UK) were used to analyse the specific surface area and PSD of CEM II and RHA, respectively. Also, XRF (Bruker AXS S4, Explorer, Germany), XRD

Table 3. Mix constituents of HPC with RHA.

Constituents	Mix Blends (kg/m^3)						
	Control	RHAC-5	RHAC-10	RHAC-15	RHAC-20	RHAC-25	RHAC-30
Water	156	156	156	156	156	156	156
Cement (CEM II)	540	513	486	459	432	405	378
RHA	0	27	54	81	108	135	162
Coarse aggregate	1050	1050	1050	1050	1050	1050	1050
Sand (≥300 um)	700	700	700	700	700	700	700
SAP (0.3% b_{wob})	1.62	1.62	1.62	1.62	1.62	1.62	1.62
Superplastiser (1.5% b_{wob})	8.10	8.10	8.10	8.10	8.10	8.10	8.10
Water/binder (W/B)	0.30	0.30	0.30	0.30	0.30	0.30	0.30
Additional Water	20.30	20.30	20.30	20.30	20.30	20.30	20.30

*W/B = ((water + liquid content of superplasticiser)/(cement + RHA).

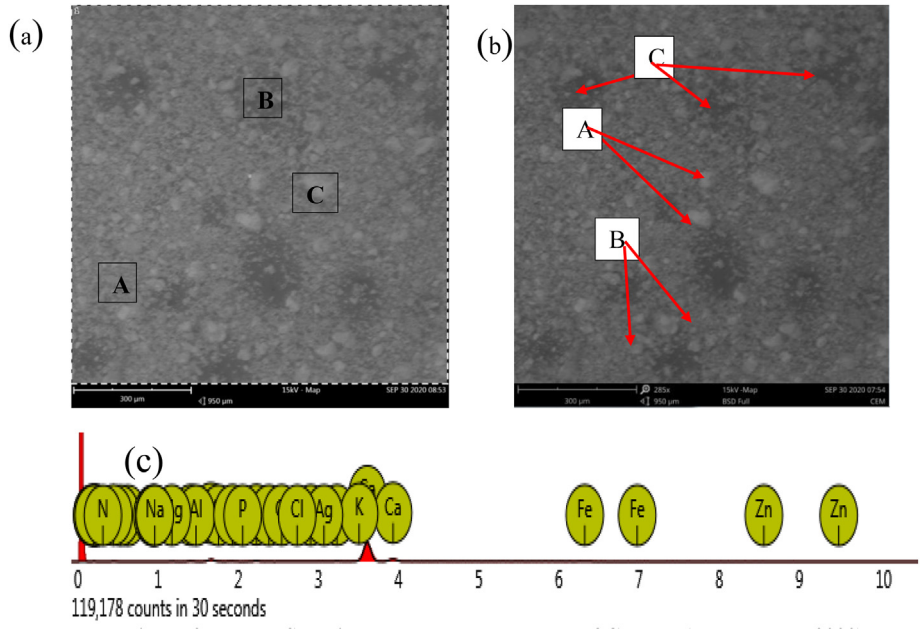

Figure 2. a–c: The SEM images and EDX patterns of CEM II (Nduka et al., 2022).

(Rigaku Miniflex 600, Washington, DC, USA), and SEM (Phenom ProX, PhenomWorld Eindhoven, The Netherland) were used to study the chemical oxides, mineralogical compositions and the morphology of the CEM II and RHA, respectively. The understanding of the functional groups was carried out with FTIR/ATR (Cary 630, Agilent Technologies, Penang, Malaysia).

2.4.2. Workability

To determine the workability of the HPC mixtures, slump flow measurement was performed using the flow table test described in EN B. 12350-5 (2009). After meeting Neville's (2012) recommendation on 400–600 mm slump flow spread on workability and cohesion for HPC. The specimen was prepared following Olawuyi's (2016) HPC preparation procedures. The cast concrete samples were covered in the laboratory with a jute bag and allowed to harden for 24 h before demoulding and curing in a water tank at 21 ± 2 °C until testing.

2.4.3. Density and porosity of HPC

The demoulded density and total porosity, n (%) of the various HPC samples using 100 mm cubes, were computed. Hence, the "designed density, *dd* and "demoulded density" *dmd* of HPC mixtures with RHA were studied. The "*dd*" was calculated by the addition of the weight of the SAP and added water for SAP absorption to the original computed weight in kg/m^3 for the control mixtures. The "*dmd*" was ascertained by dividing the direct weight of the demoulded concrete with the measured volume of a particular concrete cube. Afterwards, total porosity, n (%), was calculated using Eq. (1).

$$\text{Total porosity, n (\%)} = \frac{\text{dd} - \text{dmd}}{\text{dd}} \times 100 \quad (1)$$

Where "*dd*" is the design density, and "*dmd*" is the demoulded density.

2.4.4. Mechanical properties

2.4.4.1. Compressive strength. A total of 210 samples were prepared based on five curing ages and triplicate samples per age crush. The average triplicate sample value for compressive strength determination was done using a 2000 kN maximum loading capacity digitised materials testing machine (Model YES-2000, Eccles Technical Engineering Ltd., England) with an applied loading rate of 0.1 N/mm^2. The samples were tested for 7, 28, 56, and 90 days after curing. The compressive strength (f_c) is calculated using Eq. (2):

$$fc = \frac{F}{Ac} \quad (2)$$

where f_c is the compressive strength of the HPC mixture, MPa; F is the maximum load at failure, kN; Ac is the specimen area, mm.

2.4.4.2. Splitting tensile strength. Similarly, 126 cylinders were prepared for splitting tensile strengths determinations into four levels of curing age and three tested samples per age. The splitting tensile strength determination was carried out with the material testing equipment used for compressive strength after curing for 28, 56 and 90 days. The splitting tensile strength was computed based on the linear elastic theory defined in Eq. (3).

$$\sigma_t = \frac{2P}{\pi DL} \quad (3)$$

where σ_t is the splitting tensile strength of HPC mixtures, MPa; P is the failure load, kN; D is the specimen's diameter, mm and Lis the length of the specimen, mm.

2.4.4.3. Flexural strength. Finally, 126 beam prisms for flexural strengths determinations based on four levels of curing age and three tested samples per age were prepared. The average triplicate flexural strengths values were obtained with a manually operated three-point contact 50 kN Impact AO 320 flexural machine after 28, 56 and 90 days of curing. Flexural strength is expressed in the modulus of rupture, as shown in Eq. (4).

$$\text{MR} = \frac{3\text{PL}}{2\text{bd}^2} \quad (4)$$

where MR is the Modulus of rupture of HPC mixture, MPa; P is the failure load, kN; L is the length of the specimen, 400 mm; b is the breath of the specimen, 100 mm and d is the depth of the specimen, 100 mm.

2.4.5. Quantitative and qualitative analysis of hydration products

XRD (Kα reflections) was conducted on finely ground and homogenised HPC samples to examine the samples' crystalline phases and hydration products. The scan range of 2°–75° with two-theta steps of 0.026261 at 8.67 s per step was adopted. The powdered sample was filled in the middle of the sample holder and spread around using the front-loading technique. The glass slide was then used to press the sample to flush with the sample holder. The sample holder was loaded sideways into the XRD, and an adjustment was made upward to have the sample in firm contact with the equipment. The investigation of the hydration products and semi-quantitative chemical elements was further conducted on broken samples of the specimen coated with sputter coater by Quorum Technologies (Model Q150R) with 5 nm of gold using SEM/EDX at 200 μm magnifications. The purpose of the gold coating is to make the non-conductive materials conductive.

3. Results and discussions

3.1. Characterisation of binders

3.1.1. SEM/EDX

Figures 2a-c depict the 100 μm and 200 μm magnified CEM II SEM images utilised in this research. The images are asymmetrical, almost angular, and interconnected.

The SEM image result regarding the colour bands and morphology of this material have been discussed in an earlier publication by Nduka et al. (2022). The EDX spectra revealed calcium as the major elemental constituent and oxygen, silica and iron as the minor constituents.

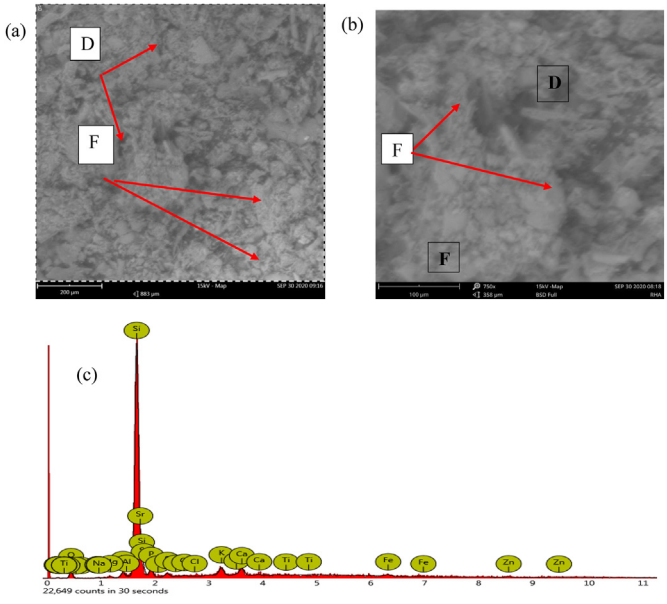

Figure 3. a–c: Sem images and EDX patterns of RHA (Nduka et al., 2022).

Table 4. EDX atomic and weight concentration of binders.

Element symbol	Element name	CEM II		RHA	
		Atomic conc.	Weight conc.	Atomic conc.	Weight conc.
Si	Silicon	5.11	4.02	55.74	54.64
Ca	Calcium	68.54	77.02	3.12	4.36
O	Oxygen	14.33	7.00	22.14	12.37
Sr	Strontium	0.00	0.00	2.66	8.15
Fe	Iron	2.09	3.20	1.40	2.73
Al	Aluminium	1.32	1.20	1.40	1.32
K	Potassium	1.32	1.22	3.29	4.49
Na	Sodium	0.20	0.13	0.49	0.40
N	Nitrogen	1.70	0.67	0.54	0.26
Ti	Titanium	0.00	0.00	0.00	0.00
Ag	Chlorine	0.37	0.46	0.47	0.58
S	Sulfur	1.67	1.65	1.49	1.67
P	Phosphorus	0.87	0.75	4.38	4.73
Mg	Magnesium	0.87	0.69	0.68	0.58
C	Carbon	0.61	0.21	0.68	0.29
Zn	Zinc	1.00	1.78	1.50	3.43
Total		100.00	100.00	99.98	100.00

The EDX spectra show silica in high content while oxygen and strontium are moderate. The investigated RHA sample has low phosphorus, potassium, and calcium contents. Table 4 shows the atomic and weight concentrations of CEM II and RHA used in the experimental study. CEM II has higher calcium (68.54%; 77.02%), oxygen (14.33; 6.43%) and silicon (5.11%; 4.02%) atomic and weight concentrations than any other elements. On the other hand, RHA mostly manifested in silicon (55.74%; 54.64%), oxygen (22.14; 12.34%) and strontium (2.66%; 8.15%) in both atomic and weight concentrations. These results complied with XRF quantitative analysis.

3.1.2. XRD

Figure 4 depicts the diffractograms of CEM II at the temperature of manufacture, with reflections of mineral content pointed out in Nduka et al. (2022). The studied result is coherent with the chemical composition data of Portland cement (Saxena et al., 2020).

Figure 5 depicts the phase structure of RHA, emphasising the mineral constituents found in previous work by Nduka et al. (2022). The XRD analysis verifies that SiO_2 is the predominant chemical oxide, as determined by XRF. The results indicated that calcining RHA to 700 °C might yield an amorphous substance (76%) suited for concrete enhancements.

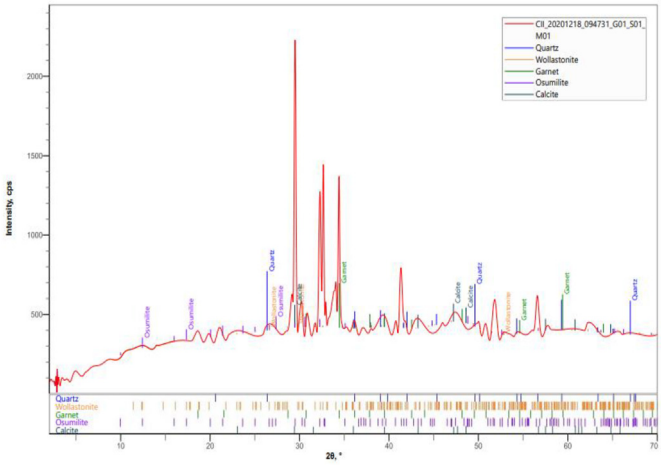

Figure 4. XRD pattern of CEM II (Nduka et al., 2022).

3.1.3. FT-IR/ATR

The FTIR bands of CEM II as shown in Figure 6 have been discussed in the previous publication of Nduka et al. (2022). The result conformed to Shrestha's (2018) findings.

Figure 7 depicts the obtained RHA-characterised IR spectra. Peak recognition was conducted based on Nascimento (2020). According to Nascimento (2020), at 3431 cm^{-1} bands, OH groups of silanois (Si–OH) and siloxanes (Si–O–Si–OH) exist, while the vibrations of asymmetric Si–O–Si stretch are linked to the intense absorption band at 1096 cm^{-1}. It was further pointed out that the vibrations of symmetrical stretching of Si–O–Si are recorded at 793 cm^{-1} and 467 cm^{-1} bands, showing the Si–O type connection. The crystalline cristobalite indicating a weak absorption phase is usually seen at 619 cm^{-1} bands. The figure indicated the absence of the symmetric and asymmetric OH stretching of 3500–3000 cm^{-1}. The stretching of O–Si–O deformation is represented at 1066 cm^{-1}, 794 cm^{-1} and 726 cm^{-1} bands. All spectra match those noticed in the scientific literature (Sembiring, 2019; Nascimento, 2020).

3.1.4. TGA

The calcination efficiency of the RHA specimen was investigated and presented in Figure 8. This factor is an important indicator of the temperature to which the raw RHA specimen was thermally treated. The TGA measurement shows that at about 300 °C, the absorbed water in the RHA's interlayer space dehydrated. It was also noticed that a further dehydroxylation of RHA mineral took place at a temperature between 350 °C to 450 °C. Also, at 560 °C, total dehydroxylation of RHA minerals occurred. Finally, at about 670 °C, the TGA curve remains undulating up to 881 °C. This point shows the maximum calcination temperature of the RHA. This result supports Makul's (2020) findings, which calcined RHA at a controlled incinerator between 500 to 700 °C for 1 h produces amorphous RHA. Therefore, it can be inferred that the studied RHA sample calcined to a maximum temperature of 670 °C remains relevant for cement replacement in HPC application.

3.2. Fresh and hardened properties of HPC

3.2.1. Slump flow

Figure 9 depicts the results of a slump flow test performed on RHA-containing HPC mixtures.

The result of the slump flow as shown in the figure has been discussed in Nduka et al. (2022) earlier study.

3.2.2. Density and porosity of HPC

The mean dry density of the reference and activated HPC samples containing RHA varies from 2390 kg/m^3 to 2308 kg/m^3 for all CEM II replacements, as presented in Figure 10. It was shown on all curing days that the dry densities of HPCs containing RHA reduced by 3.01% as the curing age increased compared with the control. Also, the comparison of different HPC mixtures containing RHA depicts that 20%, 25% and 30% replacement demonstrated lower densities than samples with 5%, 10% and 15% or no RHA. Olutoge and Adesina (2019) study reported a reduction in density when RHA content is increased in concrete application. Similarly, in his review, Thomas (2018) pointed out that low W/B (0.30–0.34) concrete made with superplasticiser and higher binder content with RHA results in highly workable concrete and cohesive mix devoid of segregation. It was further mentioned that the addition of higher RHA decreases concrete density. The result reported now agrees with the literature's deductions on densities of RHA-blended cement (Thomas, 2018; Olutoge and Adesina, 2019; Siddika et al., 2021).

3.2.3. Porosity of HPC

Table 5 depicts the design density, demoulded density and total porosity computed from seven HPC samples containing RHA. The porosity of HPC samples modified with RHA was assessed using the analytical formula, as reported in Olawuyi (2016), and the outcome is reported in Table 5.

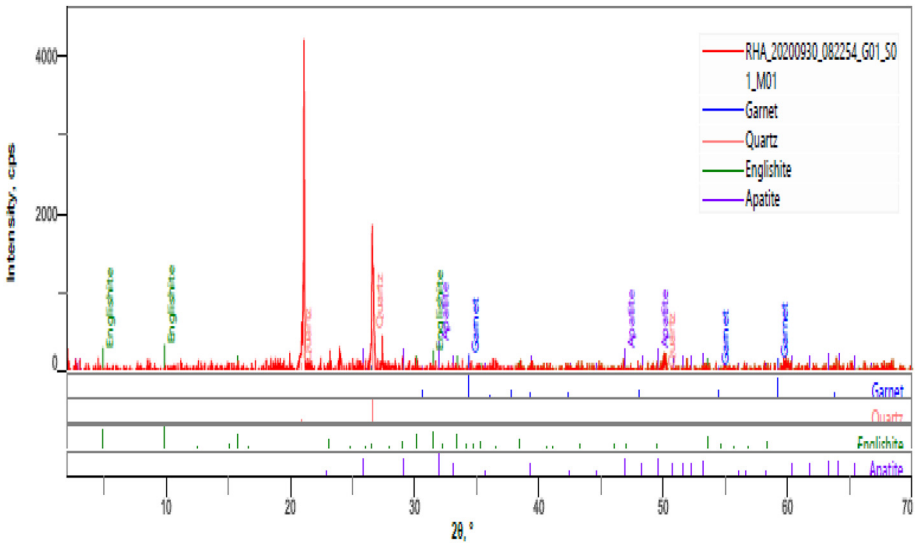

Figure 5. XRD pattern of RHA (Nduka et al., 2022).

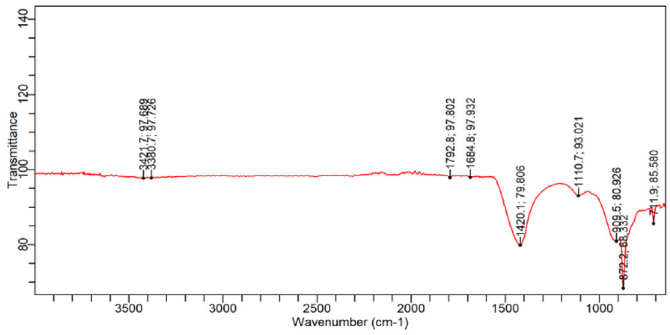

Figure 6. FTIR pattern of CEM II (Nduka et al., 2022).

From the results, RHAC-10 mixture concrete exhibited the lowest porosities of 2.38% (7 days), 2.30% (28 days), 2.26% (56 days), and 1.98% (90 days), respectively, among all the internally cured RHA modified HPC samples and much lower than the control. The results may be credited to the combined filler effect and RHA's pozzolanic upshot (Thomas, 2018). Other RHA-modified HPCs recorded higher porosity when compared with the control. Mosaberpanah and Umar (2020) reported similar porosity of 7.63% (7 days), 5.76% (28 days) and 4.92% (91 days) in their review with ultra-high-performance concrete with 20% cement substitution with RHA. Therefore, the results demonstrated that RHA used in this work exhibited a filler effect, as confirmed by the Mosaberpanah and Umar (2020) review.

3.2.4. Compressive strength

Figure 11 depicts that the control's compressive strength of RHA's blend mix varied between 37.51 and 54.47 MPa from 7 to 90 days. On the other hand, HPC's compressive strength with RHA ranged between 34.18 – 43.13 MPa for 7 days, 39.28–47.33 MPa for 28 days, 41.81–61.97 MPa for 56 days and 45.83–66.78 MPa for 90 days, respectively. These outcomes wholly depend on the replacement level and hydration age. At 7 days, 5–20 % (RHAC-5 to RHAC-20) replacement level compressive strength development was higher than control, while 25–30% (RHAC-25 to RHAC-30) replacements were observed to be lower than the control. At 28 days of curing age, only RHAC-10 compressive strength outperformed that of the control mix. Undoubtedly, as the curing days increase, the strength values also appreciate significantly. For example, at the age of 56 and 90, RHAC-5 and RHAC-10 compressive strength surpass that of control. 56-day compressive strength was recorded as 54.91,

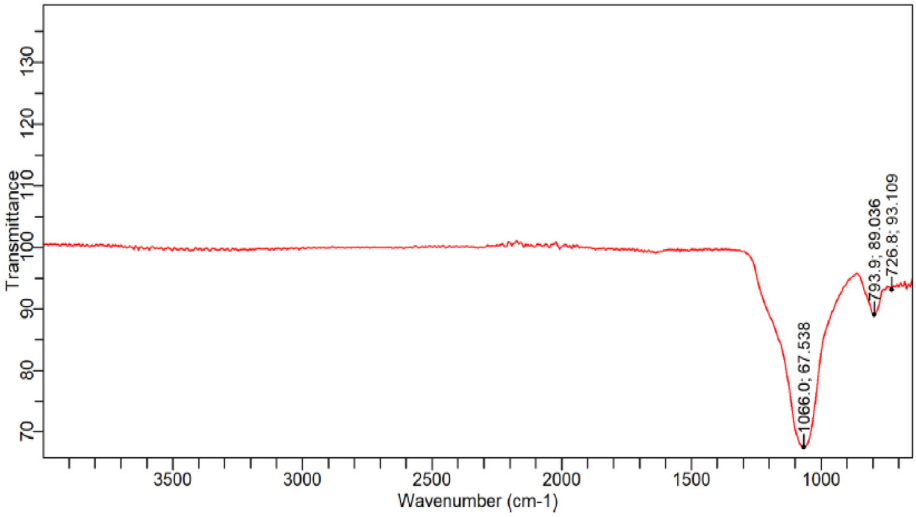

Figure 7. FTIR pattern of RHA.

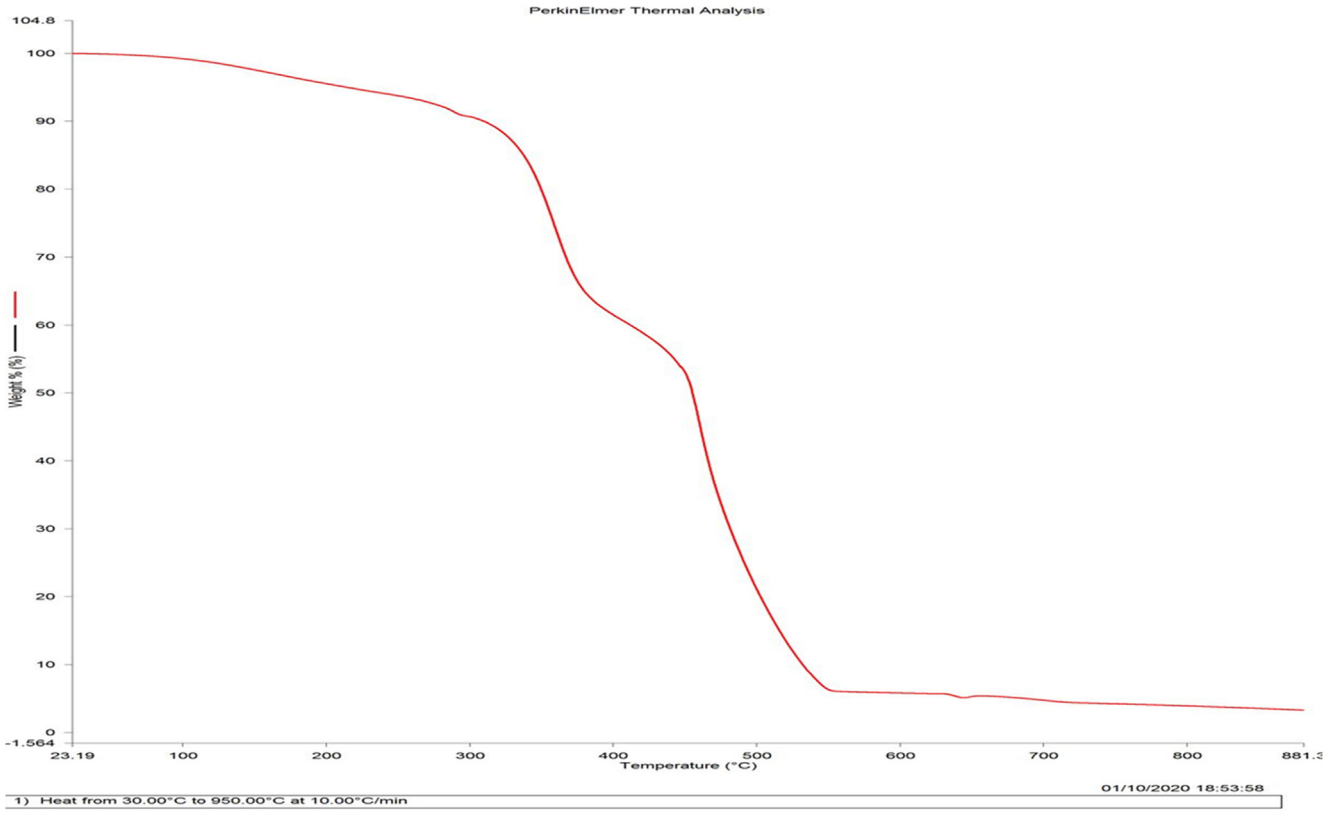

Figure 8. FTIR pattern of RHA.

61.97, 50.46, 47.66, 44.99 and 41.81 MPa for RHAC-5, RHAC-10, RHAC-15, RHAC-20, RHAC-25 and RHAC-30, respectively. A similar trend was also observed in 90 days of compressive strength, with RHAC-5, RHAC-10, RHAC-15 and RHAC-20 HPCs having a higher strength value. This result validates RHA's pozzolanic and microfilling effects, which enhance concrete's microstructure and pore structure in the bulk paste and interfacial transition zone reactivity, especially at a later age and the RHA fineness attributes (Safiuddin et al., 2010).

The figure observed that the 10% replacement mix (RHAC-10) recorded the highest compressive strength in all the curing ages with 11.69%, 18.22%, 28.73%, and 31.80% increase over the control at 7, 28, 56 and 90 days. The result implied that 10% CEM II replacement with RHA is optimum for realising HPC. The lowest compressive strength was also observed for RHAC-30 at all ages. Interestingly, all the HPCs activated with RHA could not reach the target design strength of Class 1 (50–75 MPa) at 28 days, while further curing for 56 and 90 days exhibited promising results. Mosaberpanah & Umar (2020) averred that RHA blended in PC for HPC application is expected to produce compressive strength of 55 and 72 MPa at 7 and 28 days, respectively.

Compared with other researchers' results, blended PC with RHA and similar chemical admixtures will establish the present study's produced calcined RHA's relevance. Safiuddin, West, and Soudki (2010) found 15% PC substitution with RHA optimum to achieve improved hardened properties of self-consolidating HPC. The authors achieved 98.4 MPa compressive strength concrete at 56 hydration days using the CEM I cement class as the main binder at a W/B of 0.35. Similarly, Zareei et al. (2017) found a positive relationship between 15% RHA and 10% micro

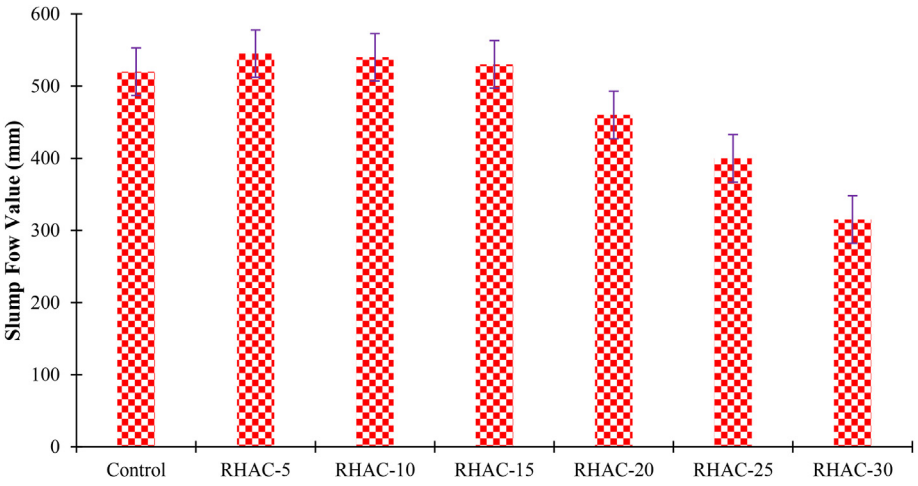

Figure 9. Slump flow of HPC made with different contents of RHA (Nduka et al., 2022).

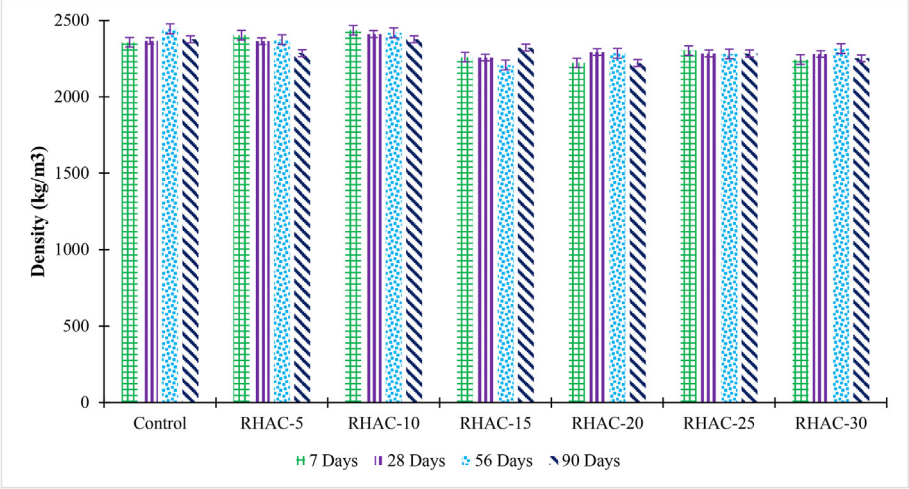

Figure 10. Density of HPC made with different contents of RHA.

Table 5. Porosity of HPC samples containing RHA.

Specimen/Age (days)	Design density, dd (kg/m^3)				Demoulded density, dmd (kg/m^3)				Total porosity, n (%)			
	7	28	56	90	7	28	56	90	7	28	56	90
Control	2476	2476	2476	2476	2346	2366	2446	2377	5.25	4.44	1.17	4.00
RHAC-5	2476	2476	2476	2476	2399	2401	2422	2425	3.11	3.10	2.18	2.05
RHAC-10	2476	2476	2476	2476	2417	2419	2420	2427	2.38	2.30	2.26	1.98
RHAC-15	2476	2476	2476	2476	2340	2345	2349	2355	5.49	5.29	5.13	4.89
RHAC-20	2476	2476	2476	2476	2349	2344	2346	2345	5.13	5.33	5.25	5.29
RHAC-25	2476	2476	2476	2476	2303	2284	2281	2283	6.99	7.75	7.88	7.80
RHAC-30	2476	2476	2476	2476	2244	2280	2315	2325	9.37	7.92	6.50	6.10

silica contents and the best compressive strength of concrete (93.28 MPa) at 28 days with a W/B ratio of 0.4%. Their best-performing concrete was 20% higher than the control concerning compressive strength. Chao--Lung et al. (2011) also found the usefulness of adding carbon-infused RHA blended concrete in obtaining Grade One HPC after 28 and 90 curing days. Therefore, these studies' findings are consistent with the present study's findings.

On the other hand, figure A-1 in the Appendix depicts that the mean compressive strength of RHA blended HPC (RHAC-5 – RHA-10) increased as the RHA contents increased. Conversely, as shown in the Figure, HPC mixtures of RHAC-15 and MCCC-30 compressive strength decreased as the RHA contents increased. This result is consistent with Sandhu and Siddique's (2017) findings on 10–15% optimum cement replacement with RHA in concrete. The lower mean compressive strength values obtained from higher substitution agree with the expectation since higher RHA content in cement blend produced lower strength in concrete. Generally, there is an increase in the mean compressive strength of RHA blended HPCs across the curing ages.

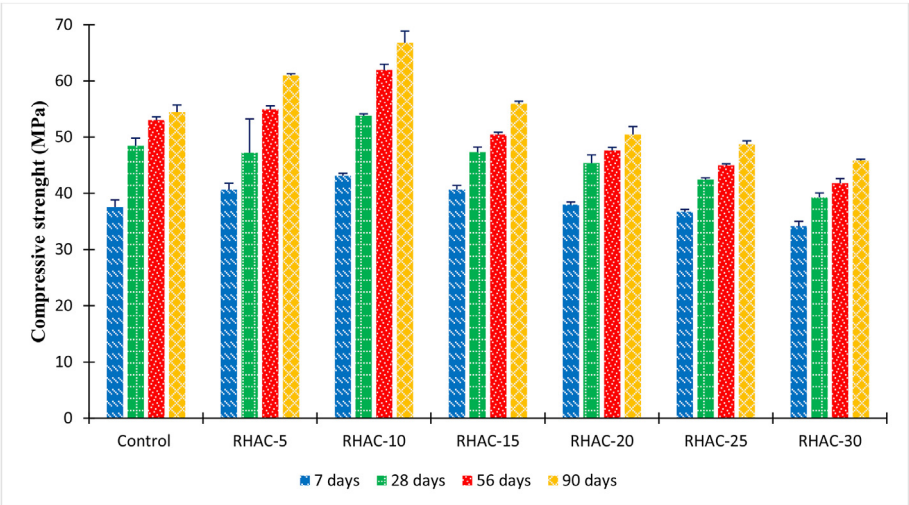

Figure 11. Compressive strength development of RHA-based HPC.

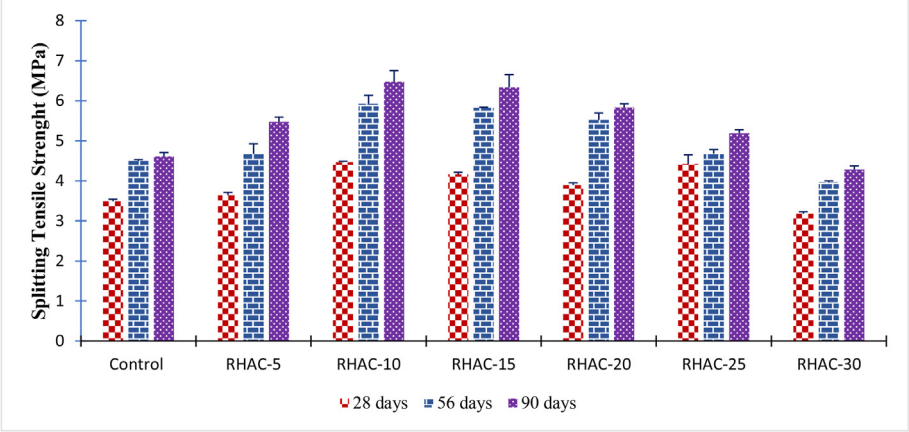

Figure 12. Splitting tensile strength results of HPCs at different treatments with RHA.

3.2.5. *Splitting tensile strength of HPCs with RHA*

RHA blended HPC's splitting tensile strength determined by the indirect diametric compression test at seven treatment conditions (0, 5,10, 15, 20, 25 and 30%) independent of the hydration time up to 90 days is shown in Figure 12, respectively.

Figure 12 demonstrates that increasing the RHA content significantly increases the splitting tensile strength of the RHA-modified HPC. For the 28 hydration days, the variation in the strength between 5 to 25% cement replacement is higher than the control. For 56 curing days, the splitting tensile strength regularly increased in line with the cement replacement level except for 30% cement replacements. The 56 days of hydration recorded 4.71, 5.94, 5.83, 5.42, 5.72 and 3.96 MPa for RHA-5 to RHAC-30 over the control with 4.50 MPa. The strength value at 90 days continues to improve considerably under all the RHAC mixes. Meanwhile, the strength value of the RHAC-10 sample increased the most for all the tested samples revealing a ~30% increase over the control samples. RHAC-5, RHAC-15, RHAC-20, RHAC-25 recorded increased strength values of ~16%, 27%, 21% and 11. 37% over the control mixture. However, the RHAC-30 sample decreased strength by 7.17% compared to the control mix. The RHA-modified HPC sample's strength value at 10–20% replacement tested at later days always exceeds plain cement (Mosaberpanah & Umar, 2020). These findings agree with the pozzolanic reactivity of RHA in cement paste found in the literature (Zareei et al., 2017; Mosaberpanah &Umar, 2020).

3.2.6. *Flexural strength of HPCs with RHA*

Flexural tensile strength (modulus of rupture) results of HPCs at different treatments with MCC or RHA are presented in Figure 13. The figure detailed HPC mixtures' flexural strength with different calcined RHA at 28, 56 and 90 days of hydration. It is clear that at 28 days of hydration, the flexural strength of the HPCs with RHA is higher than the reference mix due to pozzolanic reactivity.

The RHAC-10 had the highest flexural strength (1.48 MPa) among all the mixes induced with RHA and the reference mix (1.11 MPa). At 56 and 90 days, the flexural strength of HPC with RHA continued to increase more than the reference mix. RHAC-10 continued to dominate in strength (1.61 MPa; 1.76 MPa), followed by RHAC-15 (1.61 MPa). Interestingly, only RHAC-30 with 30% cement replacement had the lowest flexural strength than the control mix. This phenomenon may be a result of higher cement replacement with RHA causing reduced hydration products like C_3S. This result is consistent with the compression and splitting tensile test results and conforms to the positions of Safiuddin et al. (2010), Zareei et al. (2017), Mosaberpanah & Umar (2020) on the pozzolanic reactivity and filler effects of RHA on concrete and mortar.

The general linear model -Multivariant analysis obtained by SPSS v 25 showed the effects of RHA content and curing age on the compressive strength, splitting tensile and flexural strengths of RHA-based HPC mixtures. The significance is assessed based on $\propto >$ 0,0005. Table B-1 in the Appendix shows that a single factor's compressive, splitting tensile and flexural strengths significantly affect the RHA content and curing age. However, Table B-2 in Appendix depicts that single-factor analysis showed that curing age and RHA content affect flexural strength (red highlighted in Table B-2). Also noted were the no significant effects of two combinations of curing age * RHA content on compressive, splitting tensile and flexural strengths (grey colour highlighted in Table B-2).

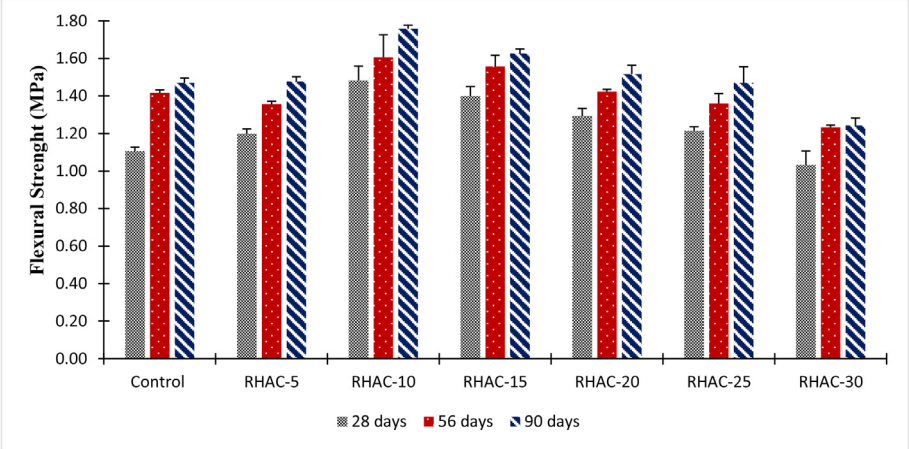

Figure 13. Flexural strength of HPCs at different treatment conditions with RHA.

3.3. Quantitative and qualitative analysis of hydration products

3.3.1. SEM analysis

On identified HPC samples (control, 10%, and 20%), SEM/EDX was used to quantitatively and qualitatively evaluate the hydration products and molecular structures of the tested samples. Figures 14, 15, and 16 depict the SEM micrographs viewed at 200 μm magnification for the control, RHAC-10, and RHAC-20 specimens at 90 days. Figure 13 depicts the SEM image of the control HPC mixture, which reveals the internal morphology and crystalline structure of the HPCs. In general, the gray-scale facilitates the identification and analysis of specific elements for a precise chemical composition evaluation. . The item designated 1 is coarse aggregate, which is dark grey in colour, large, and irregular. The portion labelled 2 reflects the angular, darker-coloured sand surrounding the coarse aggregate. On the surface of the matrix of cement paste is the light-grey background part, designated 3.

To understand the resulting hardening and microstructure of HPCs containing RHA, SEM examination revealed the microstructure of the RHAC-10 and RHAC-20 mixes after 90 days of internal curing with SAP. The SEM micrographs are in Figures 14 and 15, respectively. The figures indicate the presence of bright grey coarse aggregate with irregular shapes bordered by darker angular-shaped sand. The cement paste matrix highlights the light grey and dark grey fragments of the background that are dispersed across the hydration product surfaces. These results are consistent with the RHA-blended matrix in Thomas's (2018) and Mosaberpanah and Umar's (2020) reviews.

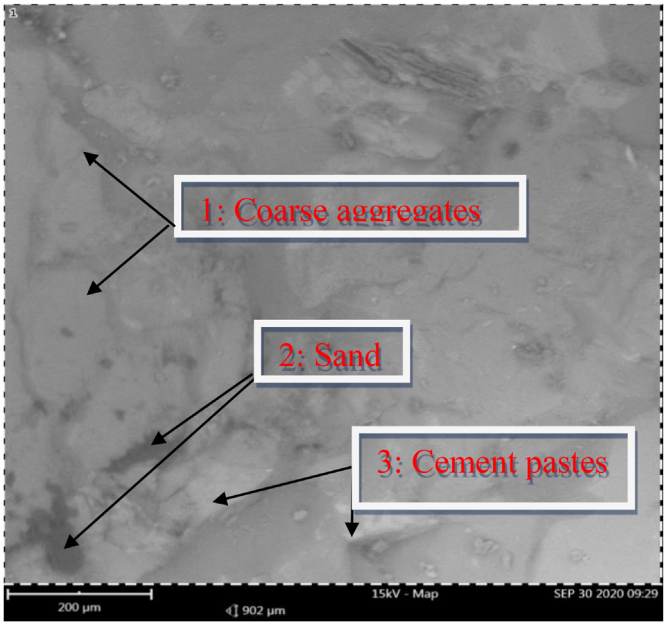

Figure 14. SEM micrograph of control HPC at 90 days.

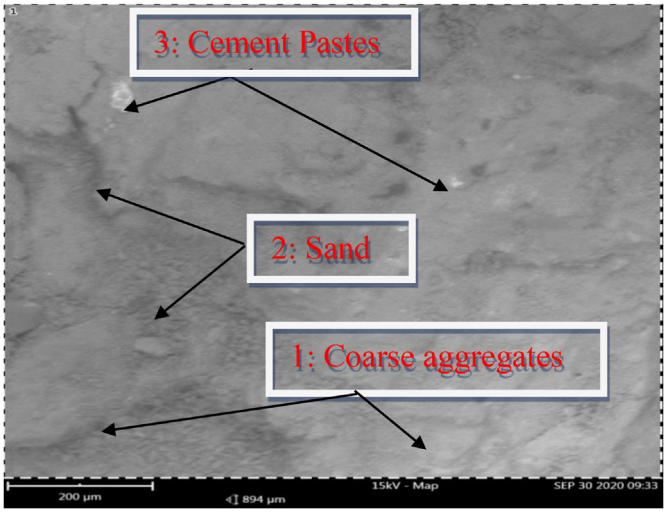

Figure 15. SEM micrograph of RHAC-10 HPC at 90 days.

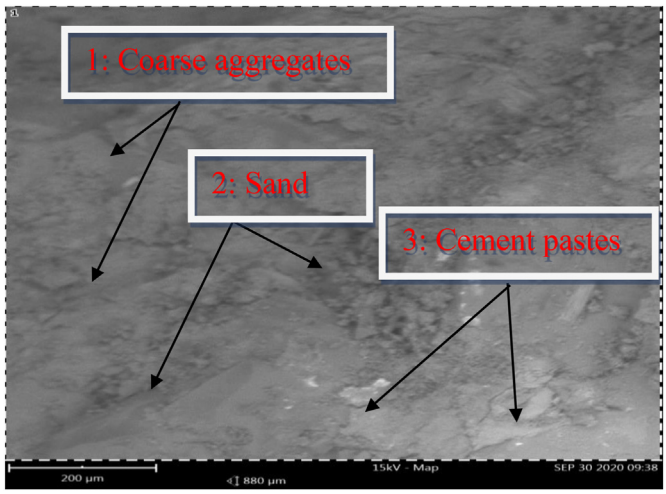

Figure 16. SEM micrograph of RHAC-20 HPC at 90 days.

Furthermore, the EDX result in Table 6 revealed each element's atomic and weight % concentrations in the mixture. The table revealed silicon (34.35%; 32.48%), calcium (18.78%; 25.35%), oxygen (22.24%; 11.98%) and aluminium (10.20; 9.26%) to be prominent in the mixture. In contrast, potassium residues (2.94%; 3.26%) and sodium (2.59%; 2.00%) were detected in the elements' phases.

The EDX result highlighting the atomic and weight concentrations % of RHAC-10 and RHAC-20 revealed the most dominating elements in Table 6. Calcium (53.07%; 63.90%); silica (13.94%; 11.74%) and oxygen (21.62%; 10.37%) showed higher concentrations than other elements found in the RHAC-10 mixture. Similarly, calcium (51.35%; 62.73%); silica (13.75%; 11.81%) and oxygen (21.26%; 9.87%) equally exhibited higher concentrations than other elements found in the RHAC-20 mixture. These results point to C–S–H hydrates and portlandite formation in the RHA-blended HPC mixtures. Compared to the reference mix, the higher calcium formation in the RHA-modified HPCs after 90 days of internal curing signifies portlandite creation.

3.3.2. XRD analysis

The XRD diffraction configurations were utilised to evaluate the crystalline phase in the hardened HPC pastes and the amount of crystalline phase at 90 days of hydration. Figures 17, 18, and 19 illustrate the XRD configurations of control and RHA-modified HPCs.

XRD analysis from Figure 16 presents the XRD configuration of control HPC hardened paste at 90 days. From the Figure, quartz (SiO_2), calcite ($CaCO_3$), portlandite ($CaO.H_2O$), phlogopite (K Mg_3(Al Si_3O10) (OH) Fe…), biotite (K, H)2(Mg. Fe^{+2})2(Al…), andradite (Ca3 $Fe_2(SiO_4)3$ are the vital crystalline phases of the hardened paste. Due to the carbonation of the constituent materials during production and sample preparation, calcite showed the highest crystalline phase (16%). Quartz, phlogopite, and biotite had respective crystalline phase contents of 8%, 7%, and 5%. At 3% and 2%, respectively, Portlandite and Andradite had the lowest crystalline phase percentages. Therefore, the mineral compositions identified by XRD analysis are representative of a calcined RHA-blended cement.

Table 6. EDX atomic and weight concentration HPCs at 90 days.

Element symbol	Element name	Control		RHAC-10		RHAC-20	
		Atomic conc.	Weight conc.	Atomic conc.	Weight conc.	Atomic conc.	Weight conc.
Si	Silicon	34.35	32.48	13.94	11.74	13.75	11.81
Ca	Calcium	18.78	25.35	53.07	63.77	51.35	62.73
O	Oxygen	22.24	11.98	21.62	10.37	21.26	9.87
Fe	Iron	5.11	9.61	3.43	5.74	4.43	6.74
Al	Aluminium	10.20	9.26	2.19	1.77	2.14	1.78
K	Potassium	2.94	3.86	1.64	1.93	1.97	1.75
Na	Sodium	2.59	2.01	0.31	0.21	0.73	0.51
Ti	Titanium	1.12	1.82	0.00	0.00	0.00	0.00
Ag	Silver	0.49	1.82	0.56	1.82	0.77	1.96
S	Sulfur	0.51	0.55	1.37	1.32	1.28	1.23
P	Phosphorus	0.52	0.54	0.71	0.65	0.80	0.71
Mg	Magnesium	0.62	0.51	0.70	0.51	0.98	0.70
C	Carbon	0.53	0.21	0.46	0.17	0.54	0.21
Zn	Zinc	0.00	0.00	0.00	0.00	0.00	0.00
Total		100	100	100	100	100	100

Figures 18 and 19 show the XRD configuration of RHAC-10 and RHAC-20 at 90 days of hydration. After 90 days of hydration, portlandite crystals were observed to be decreased to 2% for RHAC-10 and 3% for RHAC-20. Past studies have confirmed more hydration products when portlandite is consumed (Thomas, 2018). This result further explained the improved mechanical and durability behaviours of HPCs replaced with 10–20% RHA. The 10% increased RHA amount in the HPC system produced more hydration products responsible for the strength enhancement by filling the pore spaces. Thus, with RHA's pozzolanic reaction and cement's dilution, the mixtures' portlandite peak intensity

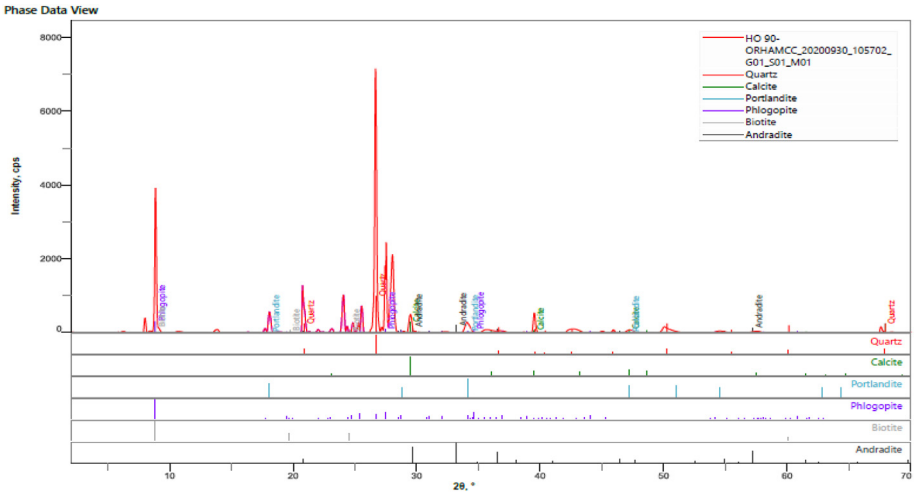

Figure 17. XRD configuration of the hardened control sample at 90 days.

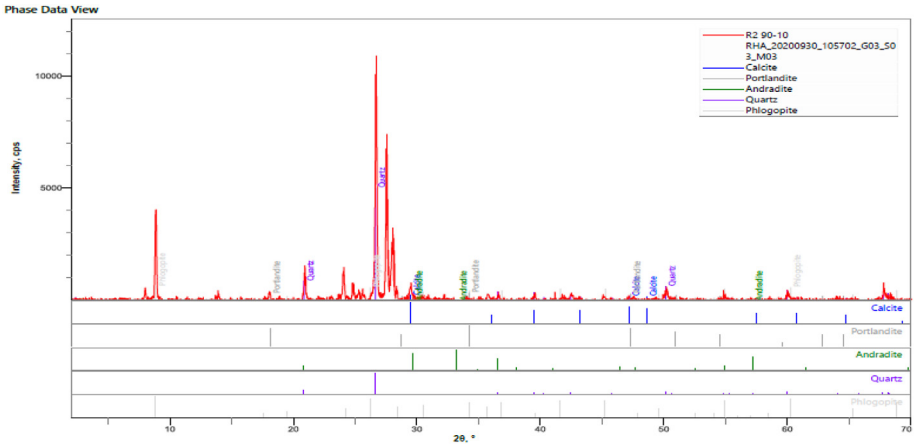

Figure 18. XRD configuration of the hardened RHAC-10 sample at 90 days.

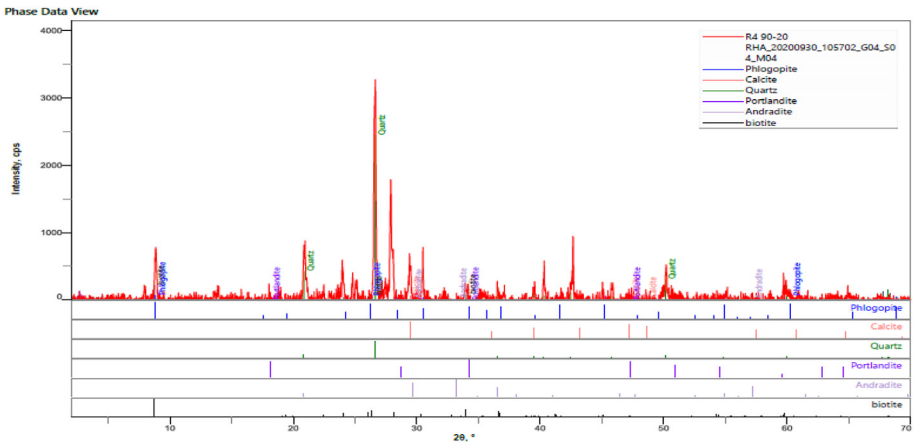

Figure 19. XRD configuration of the hardened RHAC-20 sample at 90 days.

with RHA was decreased in the later hydration period, especially with the RHAC-10 mixture.

4. Conclusion

The results of this paper on the effect of RHA on mechanical and microstructural properties of HPC internally cured with SAP can be summed up as follows:

- Only the RHAC-5 to RHAC-20 complied with the slump flow range of 450 mm–600 mm.
- The average dry density of the control and the activated HPC samples containing RHA vary from 2390 kg/m^3 to 2308 kg/m^3 and a reduction in density when RHA content is increased in HPC application.
- The greater the RHA material in HPC, the higher the porosity of HPC samples. RHAC-10 mixture recorded the least porosity. As confirmed by the pore size result (1.52 nm), RHA used in this work exhibited a close range of 2–50 nm pore structure of RHA reported by Mosaberpanah & Umar (2020) review.
- The 10% replacement mix (RHAC-10) recorded the highest compressive strength in all the curing ages implying that 10% CEM II replacement with RHA is optimum for the realisation of HPC.
- The HPC control sample's EDX atomic and weight concentrations revealed the prominent elements of silicon, calcium, oxygen, and aluminium in the mixture.
- The matrix of RHA-based cement paste highlights the background fragments of light grey and dark grey, which can be attributed to hydration products. EDX atomic and weight concentrations of RHAC-10 and RHAC-20 revealed calcium, silica, and oxygen to be the most abundant elements, respectively.
- After 90 days of hydration, portlandite crystals were observed to be decreased to 2% for RHAC-10 and 3% for RHAC-20.

Declarations

Author contribution statement

David O. Nduka, Babatunde J. Olawuyi: Conceived and designed the experiments; Performed the experiments; Contributed reagents, materials, analysis tools or data; Wrote the paper.

Emmanuel O. Fagbenle: Analyzed and interpreted the data.

Belén G. Fonteboa: Contributed reagents, materials, analysis tools or data.

Funding statement

This research did not receive any specific grant from funding agencies in the public, commercial, or not-for-profit sectors.

Data availability statement

Data will be made available on request.

Declaration of interests statement

The authors declare no conflict of interest.

Additional information

No additional information is available for this paper.

Acknowledgements

The authors are grateful to the Covenant University Centre for Research, Innovation, and Discovery (CUCRID) for its assistance with the publication of this study. Also of note are the suppliers of the superplasticiser- Masterglenium Sky 504 by BASF Limited, West Africa, facilitated by Mr Adesola Mofikoya; Superabsorbent polymers (SAP) by SNF Floerger-ZAC de Milieux, France; and Dr Charles C. Osadebe of the Nigerian Building and Road Research Institute (NBRRI), Ota, who expedited the release of 100 mm metal concrete cubes.

Appendices

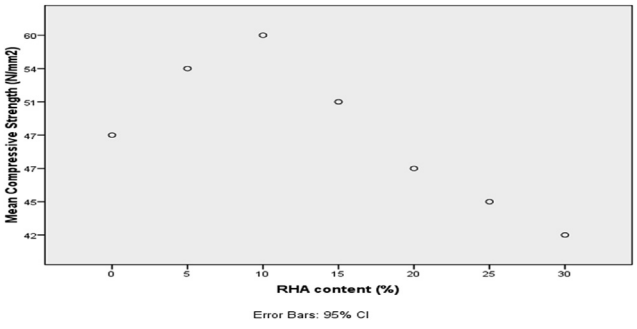

Figure A-1. Mean compressive strength of HPC against RHA contents.

Table B-1. Multivariate tests on RHA-Based mechanical properties.

Effect	Value	F	Hypothesis df	Error df	Sig.	
Intercept	Pillai's Trace	.989	2.933E3[a]	3.000	94.000	.000
	Wilks' Lambda	.011	2.933E3[a]	3.000	94.000	.000
	Hotelling's Trace	93.598	2.933E3[a]	3.000	94.000	.000
	Roy's Largest Root	93.598	2.933E3[a]	3.000	94.000	.000
Curing Age	Pillai's Trace	.585	13.095	6.000	190.000	.000
	Wilks' Lambda	.430	16.425[a]	6.000	188.000	.000
	Hotelling's Trace	1.287	19.951	6.000	186.000	.000
	Roy's Largest Root	1.258	39.852[b]	3.000	95.000	.000
RHAcont	Pillai's Trace	1.093	9.167	18.000	288.000	.000
	Wilks' Lambda	.210	10.875	18.000	266.357	.000
	Hotelling's Trace	2.347	12.083	18.000	278.000	.000
	Roy's Largest Root	1.366	21.850[b]	6.000	96.000	.000
Curing Age * RHAcont	Pillai's Trace	.526	1.700	36.000	288.000	.010
	Wilks' Lambda	.538	1.808	36.000	278.461	.005
	Hotelling's Trace	.744	1.914	36.000	278.000	.002
	Roy's Largest Root	.536	4.286[b]	12.000	96.000	.000

[a] Exact statistic
[b] The statistic is an upper bound on F that yields a lower bound on the significance level.

Table B-2. Tests of between-subjects effects RHA HPC based mechanical properties.

Source	Dependent Variable	Type III Sum of Squares	df	Mean Square	F	Sig.
Corrected Model	CS	4579.907[a]	20	228.995	8.637	.000
	STS	69.739[b]	20	3.487	11.740	.000
	FS	1.436[c]	20	.072	.738	.777
Intercept	CS	176106.668	1	176106.668	6.642E3	.000
	STS	1615.991	1	1615.991	5.441E3	.000
	FS	66.050	1	66.050	679.370	.000
Curing age	CS	1031.241	2	515.621	19.448	.000
	STS	28.791	2	14.395	48.467	.000
	FS	.035	2	.018	.182	.834
RHAcont	CS	2181.875	6	363.646	13.716	.000
	STS	33.190	6	5.532	18.624	.000
	FS	.801	6	.133	1.373	.233
Curing age * RHAcont	CS	205.143	12	17.095	.645	.799
	STS	6.345	12	.529	1.780	.062
	FS	.430	12	.036	.368	.972
Error	CS	2545.238	96	26.513		
	STS	28.513	96	.297		
	FS	9.333	96	.097		
Total	CS	282678.00	117			
	STS	2438.790	117			
	FS	105.000	117			
Corrected Total	CS	7125.145	116			
	STS	98.252	116			
	FS	10.769	116			

a. R Squared = .643 (Adjusted R Squared =.568)
b. R Squared = .710 (Adjusted R Squared =.649)
c. R Squared = .133 (Adjusted R Squared =.047)
d. R Squared = . (Adjusted R Squared = .)

References

Abalaka, A.E., 2012. Effects of method of incineration on rice husk ash blended concrete. ATBU J. Environ. Technol. 5 (1), 34–47. https://scholar.google.com/scholar?hl=en&as_sdt=0%2C5&q=Effects+of+method+of+incineration+on+rice+husk+ash+blended+concrete&btnG=.

ACI THPC/TAC, 1999. ACI Defines High-Performance concrete (The Technical Activities Committee Report. (Chairman - H.G. Russell). USA: American Concrete Institute Farmington Hills, Michigan, USA.

Afroughsabet, V., Biolzi, L., Monteiro, P.J., Gastaldi, M.M., 2021. Investigation of the mechanical and durability properties of sustainable high performance concrete based on calcium sulfoaluminate cement. J. Build. Eng., 102656

Agbede, I.O., Obam, S.O., 2008. Compressive strength of rice husk ash-cement sandcrete blocks. Global J. Eng. Res. 7 (1), 43–46.

Aïtcin, P.C., 2004. High-Performance Concrete. Taylor & Francis e-Library, New York, USA.

Alhassan, M., 2008. Potentials of rice husk ash for soil stabilization. Assumption Univ. J. Tech. 11 (4), 246–250. http://repository.futminna.edu.ng/jspui/handle/123456789/2256.

Almenares, R.S., Vizcaíno, L.M., Damas, S., Mathieu, A., Alujas, A., Martirena, F., 2017. Industrial calcination of kaolinitic clays to make reactive pozzolans. Case Stud. Constr. Mater. 6, 225–232.

Ambedkar, B., Alex, J., Dhanalakshmi, J., 2017. Enhancement of mechanical properties and durability of the cement concrete by RHA as cement replacement: experiments and modeling. Construct. Build. Mater. 148, 167–175.

ASTM C618, 2015. Standard Specification for Coal Fly Ash and Raw or Calcined Natural Pozzolan for Use in concrete. Annual book of ASTM standards, West Conshohocken, Pennsylvania, United States.

Bie, R.S., Song, X.F., Liu, Q.Q., Ji, X.Y., Chen, P., 2015. Studies on effects of burning conditions and rice husk ash (RHA) blending amount on the mechanical behavior of cement. Cement Concr. Compos. 55, 162–168.

Biskri, Y., Achoura, D., Chelghoum, N., Mouret, M., 2017. Mechanical and durability characteristics of High-Performance Concrete containing steel slag and crystalized slag as aggregates. Construct. Build. Mater. 150, 167–178.

Büyüköztürk, O., Lau, D., 2004. High Performance Concrete: Fundamentals and Application. Department of Civil and Environmental Engineering, Massachusetts Institute of Technology, Cambridge. http://bccw.cityu.edu.hk/denvid.lau/documents/HPC_Fundamentals_and_Application.pdf.

Chao-Lung, H., Le Anh-Tuan, B., Chun-Tsun, C., 2011. Effect of rice husk ash on the strength and durability characteristics of concrete. Construct. Build. Mater. 25 (9), 3768–3772.

Chindaprasirt, P., Kanchanda, P., Sathonsaowaphak, A., Cao, H.T., 2007. Sulfate resistance of blended cements containing fly ash and rice husk ash. Construct. Build. Mater. 21 (6), 1356–1361.

Dabai, M.U., Muhammad, C., Bagudo, B.U., Musa, A., 2009. Studies on the effect of rice husk ash as a cement admixture. Nigerian J. Basic Appl. Sci. 17 (2), 252–256. http://www.ajol.info/browse-journals.

De Meyst, L., Mannekens, E., Tittelboom, K.V., De Belie, N., 2021. The influence of superabsorbent polymers (SAPs) on autogenous shrinkage in cement paste, mortar and concrete. Construct. Build. Mater. 286, 122948.

De Sensale, G.R., Viacava, I.R., 2018. A study on blended Portland cements containing residual rice husk ash and limestone filler. Construct. Build. Mater. 166, 873–888.

Dushimimana, A., Niyonsenga, A.A., Nzamurambaho, F., 2021. A review on strength development of high performance concrete. Construct. Build. Mater. 307, 124865.

EN, B., 2009. 12350-5. Testing Fresh Concrete – Part 5: Flow Table Test. British Standards Institution (BSI), London,UK, pp. 1–14.

EN, B., 2010. 12390-6. Testing hardened concrete: Tensile splitting strength of test specimens. British Standards Institute, London, UK.

EN, B., 2019. 12390–3: Standard Test Method for Compressive Strength. British Standards Institute (BSI), London, UK.

EN, BS, 2011. 197-1. Composition, Specifications and Conformity Criteria for Common Cements. European Committee for Standardizations, London, England.

Faleschini, F., Fernández-Ruíz, M.A., Zanini, M.A., Brunelli, K., Pellegrino, C., Hernández-Montes, E., 2015. High performance concrete with electric arc furnace slag as aggregate: mechanical and durability properties. Construct. Build. Mater. 101, 113–121.

Fapohunda, C., Akinbile, B., Shittu, A., 2017. Structure and properties of mortar and concrete with rice husk ash as partial replacement of ordinary Portland cement–A review. Int. J. Sust. Built Environ. 6 (2), 675–692.

Ganesan, K., Rajagopal, K., Thangavel, K., 2008. Rice husk ash blended cement: assessment of optimal level of replacement for strength and permeability properties of concrete. Construct. Build. Mater. 22 (8), 1675–1683.

Gastaldini, A.L.G., Da Silva, M.P., Zamberlan, F.B., Neto, C.M., 2014. Total shrinkage, chloride penetration, and compressive strength of concretes that contain clear-coloured rice husk ash. Construct. Build. Mater. 54, 369–377.

Ghafari, E., Ghahari, S.A., Costa, H., Júlio, E., Portugal, A., Durães, L., 2016. Effect of supplementary cementitious materials on autogenous shrinkage of ultra-high performance concrete. Construct. Build. Mater. 127, 43–48.

Harbec, D., Zidol, A., Tagnit-Hamou, A., Gitzhofer, F., 2017. Mechanical and durability properties of high-performance glass fume concrete and mortars. Construct. Build. Mater. 134, 142–156.

He, Z.,A., Shen, A., Guo, Y., Lyu, Z., Li, D., Qin, X., Zhao, M., Wang, Z., 2019. Cement-based materials modified with superabsorbent polymers: a review. Construct. Build. Mater. 225, 569–590.

Igarashi, S.I., Watanabe, A., Kawamura, M., 2005. Evaluation of capillary pore size characteristics in high-strength concrete at early ages. Cement Concr. Res. 35 (3), 513–519.

International Union of Testing and Research Laboratories for Materials and Structures (RILEM), 1975. CPC4 - Compressive Strength of concrete 1975, TC14-CPC, RILEM Technical Recommendations for the Testing and Use of Construction Materials. E & FN, Spon, London, UK, pp. 17–18. https://standards.iteh.ai/catalog/standards/cen/7eb738ef-44af-436c-ab8e-e6561571302c/en-12390-3-2019.

Jaskulski, R., Jóźwiak-Niedźwiedzka, D., Yakymechko, Y., 2020. Calcined clay as supplementary cementitious material. Materials 13 (21), 4734.

Kaur, K., Singh, J., Kaur, M., 2018. Compressive strength of rice husk ash based geopolymer: the effect of alkaline activator. Construct. Build. Mater. 169, 188–192.

Li, D., Chen, B., Chen, X., Fu, B., Wei, H., Xiang, X., 2020. Synergetic effect of superabsorbent polymer (SAP) and crystalline admixture (CA) on mortar macro-crack healing. Construct. Build. Mater. 247, 118521.

Ma, Y., Shi, C., Lei, L., Sha, S., Zhou, B., Liu, Y., Xiao, Y., 2020. Research progress on polycarboxylate based superplasticizers with tolerance to clays - a review. Construct. Build. Mater. 255.

Madandoust, R., Ranjbar, M.M., Moghadam, H.A., Mousavi, S.Y., 2011. Mechanical properties and durability assessment of rice husk ash concrete. Biosyst. Eng. 110 (2), 144–152.

Makul, N., 2020. Advanced smart concrete – a review of current progress, benefits and challenges. J. Clean. Prod. 274, 122899.

Mazloom, M., Ramezanianpour, A.A., Brooks, J.J., 2004. Effect of silica fume on mechanical properties of high-strength concrete. Cement Concr. Compos. 26 (4), 347–357.

Mechtcherine, V., Wyrzykowski, M., Schröfl, C., Snoeck, D., Lura, P., De Belie, N., et al., 2021. Application of super absorbent polymers (SAP) in concrete construction—update of RILEM state-of-the-art report. Mater. Struct. 54 (2), 1–20.

Mosaberpanah, M.A., Umar, S.A., 2020. Utilizing rice husk ash as supplement to cementitious materials on performance of ultra high performance concrete: –A review. Materials Today Sustainability 7, 100030.

Nascimento, A.C.K., 2020. Study of rice husk ash by infrared spectroscopy. Int. J. Sci. Eng. Invest. 9 (101), 60–62. http://www.ijsei.com/papers/ijsei-910120-09.pdf.

Nduka, D.O., Olawuyi, B.J., Fagbenle, O.I., Fonteboa, B.G., 2022. Assessment of the durability dynamics of high-performance concrete blended with a fibrous rice husk ash. Crystals 12 (1), 75.

Nduka, D.O., Olawuyi, B.J., Mosaku, T.O., Joshua, O., 2020. Influence of superabsorbent polymers on properties of high-performance concrete with active supplementary cementitious materials of Nigeria. In: Boshoff, W., Combrinck, R., Mechtcherine, V., Wyrzykowski, M. (Eds.), 3rd International Conference on the Application of Superabsorbent Polymers (SAP) and Other New Admixtures towards Smart Concrete. SAP 2019, RILEM Bookseries, 24. Springer, Cham.

Neville, A.M., 2012. Properties of concrete, fifth ed. Pearson Educational Limited, London, England https://www.pearson.com/uk/educators/higher-education educators/program/Neville-Properties-of-Concrete-Properties-of-Concrete-5th-Edition/PGM1001873.html.

Nigeria industrial standard [NIS] 444-1, 2018. Composition, Specification and Conformity Criteria for Common Cements. Standards Organization of Nigeria, Abuja, Nigeria. https://standards.lawnigeria.com/2019/07/18/nigerian-standards-for-construction-materials-and-building-manufacturing-engineering/.

Nwankwo, C.O., Bamigboye, G.O., Davies, I.E., Michaels, T.A., 2020. High volume Portland cement replacement: a review. Construct. Build. Mater. 260, 120445.

Oh, S., Choi, Y.C., 2018. Superabsorbent polymers as internal curing agents in alkali activated slag mortars. Construct. Build. Mater. 159, 1–8.

Olawuyi, B.J., 2016. The Mechanical Behaviour of High-Performance concrete with Superabsorbent Polymers (SAP). Ph.D. Thesis, University of Stellenbosch, Stellenbosch, South Africa.

Olawuyi, B.J., Boshoff, W.P., 2013. Compressive strength of high-performance concrete with absorption capacity of Super-Absorbing-Polymers (SAP). Proceedings of the Research and Application in Structural Engineering, Mechanics and Computation, Cape Town, South Africa 978, 2–4.

Olawuyi, B.J., Boshoff, W.P., 2017. Influence of SAP content and curing age on air void distribution of high-performance concrete using 3D volume analysis. Construct. Build. Mater. 135, 580–589.

Olawuyi, B.J., Saka, R.O., Nduka, D.O., Babafemi, A.J., 2020. Comparative study of superabsorbent polymers and pre-soaked pumice as internal curing agents in rice husk ash based high-performance concrete. In: Boshoff, W., Combrinck, R., Mechtcherine, V., Wyrzykowski, M. (Eds.), 3rd International Conference on the Application of Superabsorbent Polymers (SAP) and Other New Admixtures towards Smart Concrete. SAP 2019, RILEM Bookseries, 24. Springer, Cham.

Olutoge, F.A., Adesina, P.A., 2019. Effects of rice husk ash prepared from charcoal-powered incinerator on the strength and durability properties of concrete. Construct. Build. Mater. 196, 386–394.

Oyekan, G.L., Kamiyo, O.M., 2008. Effect of Nigerian rice husk ash on some engineering properties of sandcrete blocks and concrete. Res. J. Appl. Sci. 3 (5), 345–351. https://scholar.google.com/scholar?hl=en&as_sdt=0%2C5&q=Effect+of+Nigerian+rice+husk+ash+on+some+engineering+properties+of+sandcrete+blocks+and+concrete&btnG=.

Safiuddin, M., West, J.S., Soudki, K.A., 2010. Hardened properties of self-consolidating high performance concrete including rice husk ash. Cement Concr. Compos. 32 (9), 708–717.

Salas, A., Delvasto, S., de Gutierrez, R.M., Lange, D., 2009. Comparison of two processes for treating rice husk ash for use in high-performance concrete. Cem. Concr. Res. 39 (9), 773–778.

Salisu, J., Gao, N., Quan, C., 2021. Techno-economic assessment of co-gasification of rice husk and plastic waste as an off-grid power source for small scale rice milling-an Aspen Plus model. J. Anal. Appl. Pyrol. 158, 105157.
Sandhu, R.K., Siddique, R., 2017. Influence of rice husk ash (RHA) on the properties of self-compacting concrete: a review. Construct. Build. Mater. 153, 751–764.
Saxena, S.K., Kumar, M., Chundawat, D.S., Singh, N.B., 2020. Utilization of wollastonite in cement manufacturing. Mater. Today Proc.
Schröfl, C., Erk, K.A., Siriwatwechakul, W., Wyrzykowski, M., Snoeck, D., 2022. Recent progress in superabsorbent polymers for concrete. Cement Concr. Res. 151, 106648.
Scrivener, K., Martirena, F., Bishnoi, S., Maity, S., 2018. Calcined clay limestone cements (LC3). Cement Concr. Res. 114, 49–56.
Sembiring, S., 2019. Preliminary study on functional groups characteristics of asphalt containing rice husk silica. J. Technomaterials Phys. 1 (1), 61–66. https://talenta.usu.ac.id/index.php/JoTP.
Senff, L., Modolo, R.C.E., Ascensão, G., Hotza, D., Ferreira, V.M., Labrincha, J.A., 2015. Development of mortars containing superabsorbent polymer. Construct. Build. Mater. 95, 575–584.
Shrestha, 2018. Characterization of some cement samples of Nepal using FTIR spectroscopy. Int. J. Adv. Res. Chem. Sci.
Siddika, A., Al Mamun, M.A., Alyousef, R., Mohammadhosseini, H., 2021. State-of-the-art-review on rice husk ash: a supplementary cementitious material in concrete. J. King Saud Univ. Eng. Sci. 33 (5), 294–307.
Snellings, R., Chwast, J., Cizer, Ö., De Belie, N., Dhandapani, Y., Durdzinski, P., et al., 2018. RILEM TC-238 SCM recommendation on hydration stoppage by solvent exchange for the study of hydrate assemblages. Mater. Struct. 51 (6), 1–4.
Snoeck, D., Goethals, W., Hovind, J., Trtik, P., Van Mullem, T., Van den Heede, P., De Belie, N., 2021. Internal curing of cement pastes by means of superabsorbent polymers visualized by neutron tomography. Cement Concr. Res. 147, 106528.
Snoeck, D., Jensen, O.M., De Belie, N., 2015. The influence of superabsorbent polymers on the autogenous shrinkage properties of cement pastes with supplementary cementitious materials. Cement Concr. Res. 74, 59–67.
Snoeck, D., Schröfl, C., Mechtcherine, V., 2018. Recommendation of RILEM TC 260-RSC: testing sorption by superabsorbent polymers (SAP) prior to implementation in cement-based materials. Mater. Struct. 51 (5), 1–7.
Srinath, D., Ramesh, G., Ramya, D., Krishna, B.V., 2021. Mechanical properties of sustainable concrete by using RHA and hydrated lime. Int. J. Modern Trends Sci. Tech. 7 (2).
Tan, Y., Lu, X., He, R., Chen, H., Wang, Z., 2021. Influence of superabsorbent polymers (SAPs) type and particle size on the performance of surrounding cement-based materials. Construct. Build. Mater. 270, 121442.
Tenório Filho, J.R., Mannekens, E., Van Tittelboom, K., Snoeck, D., De Belie, N., 2020. Assessment of the potential of superabsorbent polymers as internal curing agents in concrete by means of optical fiber sensors. Construct. Build. Mater. 238, 117751.
Thomas, B.S., 2018. Green concrete partially comprised of rice husk ash as a supplementary cementitious material–A comprehensive review. Renew. Sustain. Energy Rev. 82, 3913–3923.
Tu, W., Zhu, Y., Fang, G., Wang, X., Zhang, M., 2019. Internal curing of alkali-activated fly ash-slag pastes using superabsorbent polymer. Cement Concr. Res. 116, 179–190.
Tulashie, S.K., Ebo, P., Ansah, J.K., Mensah, D., 2021. Production of Portland pozzolana cement from rice husk ash. Materialia 16, 101048.
Umasabor, R.I., Okovido, J.O., 2018. Fire resistance evaluation of rice husk ash concrete. Heliyon 4 (12), e01035.
Wi, K., Lee, H.S., Lim, S., Song, H., Hussin, M.W., Ismail, M.A., 2018. Use of an agricultural byproduct, nano sized Palm Oil Fuel Ash as a supplementary cementitious material. Construct. Build. Mater. 183, 139–149.
Xu, F., Lin, X., Zhou, A., 2021. Performance of internal curing materials in high-performance concrete: a review. Constr. Build. Mater. 311, 125250.
Yang, J., Wang, F., He, X., Su, Y., 2019. Pore structure of affected zone around saturated and large superabsorbent polymers in cement paste. Cement Concr. Compos. 97, 54–67.
Zareei, S.A., Ameri, F., Dorostkar, F., Ahmadi, M., 2017. Rice husk ash as a partial replacement of cement in high strength concrete containing micro silica: evaluating durability and mechanical properties. Case Stud. Constr. Mater. 7, 73–81.
Zhang, M.H., Tam, C.T., Leow, M.P., 2003. Effect of water-to-cementitious materials ratio and silica fume on the autogenous shrinkage of concrete. Cement Concr. Res. 33 (10), 1687–1694.
Zhong, P., Hu, Z., Griffa, M., Wyrzykowski, M., Liu, J., Lura, P., 2021a. Mechanisms of internal curing water release from retentive and non-retentive superabsorbent polymers in cement paste. Cement Concr. Res. 147, 106494.
Zhong, P., Hu, Z., Griffa, M., Wyrzykowski, M., Liu, J., Lura, P., 2021b. Mechanisms of internal curing water release from retentive and non-retentive superabsorbent polymers in cement paste. Cement Concr. Res. 147, 106494.
Zhong, P., Wyrzykowski, M., Toropovs, N., Li, L., Liu, J., Lura, P., 2019. Internal curing with superabsorbent polymers of different chemical structures. Cement Concr. Res. 123, 105789.